Validation of a TLP Wind Turbine Numerical Model Against Model-scale Tests Under Regular and Irregular Waves

Mustafa Vardaroglu[a,*], Zhen Gao[b], Alberto Maria Avossa[a] and Francesco Ricciardelli[a]

[a]Università degli Studi della Campania "Luigi Vanvitelli" via Roma 29, Aversa, Italy, 81031
[b]Norwegian University of Science and Technology Otto Nielsens veg 10, NO-7491 Trondheim, Norway

ARTICLE INFO

Keywords:
TLP wind turbine
Numerical modeling
frequency-domain analyses
motion response analyses

ABSTRACT

Higher capacity factors compared to the onshore wind, decreasing cost of energy make floating wind turbines a powerful source of carbon-free energy future. Response of floating wind turbines can be observed over numerical analyses and physical model tests. In this study, the dynamic response of a TLP FWT numerical model is investigated under regular and irregular waves and compared with a scaled physical model. Open-source numerical tools are utilized in the time-domain and frequency domain. The comparison of the full-scale responses between the numerical and the experimental results are based on the use of measured waves as input to the numerical model to reduce the uncertainties in the wave simulations. Hydrodynamic damping in the numerical model is tuned according to the decay tests on the scaled physical model. Overall, close estimations of the physical model motion response, tendon tensions, and tower base moments are obtained over the comparisons of time histories, RAO, and statistics. Uncertainties in the physical model measurements and the limits of the numerical model are discussed.

1. Introduction

Tension leg platforms (TLP) are utilized in oil & gas industry in deep waters and provide stability by tensioned tendons. TLPs are advantageous for offshore wind turbine applications featuring lower displacement responses compared to the other platforms. High tension and cyclic loads on the tendons accompanied by the risk of tendon failure, complicated installation due to the deep draft height, and difficulties in towing due to the lack of additional ballast are the disadvantages of TLP wind turbines. The coupled responses of the Floating Wind Turbines (FWT) under simultaneous wind and wave loads are crucial and shall be analyzed with numerical tools or physical tests. Prototype testing reflects the harsh ocean nature and the coupled behavior of spar and semi-submersible FWTs. To the authors' knowledge, there are no existing prototype scale TLP tests.

Physical model tests are conducted to understand better the coupled behavior of FWTs and for validation purposes of numerical tools. Tomasicchio, D'Alessandro, Musci, Fonseca, Mavrakos, Kirkegaard, Katsaounis, Penchev, Schüttrumpf, Wolbring et al. (2014) conducted tests on 1:40 Froude scaled model of MIT/NREL TLP (Matha, 2010) and OC3-HYWIND spar buoy (Jonkman, 2010). The tower and the blades were scaled geometrically without considering flexibility. Free-decay, regular and irregular wave tests were conducted (Armenio and D'Alessandro, 2013). Results of the spar buoy tests have already been presented by Tomasicchio, D'Alessandro, Avossa, Riefolo, Musci, Ricciardelli and Vicinanza (2018), where effects of static mean thrust wind loading on the nacelle motions, and the effects of the rigid tower on the coupled response were discussed. Riefolo, Vardaroglu and Avossa (2018) discussed the results of wave basin tests on the TLP wind turbine, where the same tower was used with the spar buoy scaled model. Extremely small heave, pitch, and roll responses are reported from the scaled TLP model tests by Armenio (2014). Oguz, Clelland, Day, Incecik, López, Sánchez and Almeria (2018) conducted experimental and numerical studies on Iberdrola TLP concept. Thrust forces on the rotor were generated by the "software in the loop" approach. According to the results of the tests, it is reported that the wave-induced second-order forces were relatively smaller than aerodynamic forces.

Numerical computations on FWTs avoid the possible high costs and uncertainties of physical testing. Tracy (2007) conducted a parametric design study on NREL 5-MW baseline wind turbine. Accordingly, TLP, slack catenary mooring platforms, and taut catenary mooring platforms were tested. Matha (2010), Jonkman and Matha (2010) developed

*Corresponding author
mustafa.vardaroglu@unicampania.it (M. Vardaroglu)
ORCID(s):

the MIT/NREL TLP wind turbine, based on the MIT TLP#1 10-m sea state design by Tracy (2007).Hydrodynamic analyses were conducted in the frequency domain with WAMIT (Lee and Newman, 2006). Motion response analyses under the simultaneous wind and wave loading were conducted by using FAST (Jonkman, 2007). Bachynski and Moan (2012), Bachynski (2014) carried out a parametric design study on single-column TLP wind turbines. Effects of center-column diameter, pontoon radius, permanent ballast mass, water depth on the response were compared, also considering the TLP costs.

In a preliminary study, Vardaroglu, Gao, Avossa and Ricciardelli (2020) calibrated the readily available MIT/NREL TLP numerical model according to the free decay tests conducted on the scaled physical model used in Hydralab IV project (Armenio and D'Alessandro, 2013). It should be noted that pontoons (spokes) were not considered in the frequency-domain solutions.

In this paper, a numerical analysis framework is developed by using open-access tools, which is used to evaluate the response of a tension leg platform floating wind turbine under wave loads. The model is based on the MIT/NREL TLP numerical model and a scaled physical model tested in the DHI offshore wave basin within the Hydralab IV project (Armenio and D'Alessandro, 2013). This paper aims to understand the uncertainties in the physical model tests and the drawbacks of the numerical model by comparing the numerical and physical model responses. For this purpose, the computational routine used by Vardaroglu et al. (2020) is upgraded with hydrodynamic analyses conducted in the frequency domain, where the effects of the pontoons are also examined. The upgraded numerical model is equipped with measured wave elevation time series at the offshore wave basin to better estimate platform motion response, tower base, and tendon reactions of the scaled physical model in the time domain. In parallel, mean-drift loads are also taken into account to catch the low-frequency oscillations in horizontal degrees of freedom. Consequently, the numerical model is validated by comparisons with the physical model response under wave loads. Besides the differences and uncertainties of each approach, it is shown how two models also complement each other. Moreover, the risk of resonance at platform pitch natural period due to the incident waves is highlighted.

Accordingly, physical model and numerical model properties are given briefly in the following sections. Followingly, dynamic response comparisons of the physical and numerical models are discussed with highlights on the differences. Origin of the coordinate system is located at the center top of the TLP and still water level, z=0. Unless indicated otherwise, all the dimensions, properties, results, and response comparisons related to the referred structures are given in full (prototype) scale.

2. Physical modeling

In this study, the physical TLP wind turbine model that was tested in October 2012 in the offshore wave basin of Danish Hydraulic Institute (DHI) in Hørsholm, Denmark, is named as DHI TLP physical model, which was a 1:40 scaled model of MIT/NREL TLP reference design including pontoons. Tests were conducted in the scope of the Hydralab IV project (Tomasicchio et al., 2014). The main purpose of the tests was to understand the responses of two floating offshore wind turbine models under different ocean conditions and to create a database for numerical model calibration and verification purposes (Armenio and D'Alessandro, 2013). It should be noted that the pontoons (spokes) were considered massless in the MIT/NREL TLP design (Matha, 2010) except in Morison's representation. In addition to the presence of the pontoons, 25% less mooring stiffness is detected in the DHI TLP physical model compared to the original structure. Details of the physical model are given by Vardaroglu et al. (2020), Armenio and D'Alessandro (2013), Tomasicchio et al. (2014). In this study, the response of the DHI TLP scaled physical model from free decay tests is used to calibrate the DHI TLP numerical model. Response from regular and irregular wave tests are compared to the response from the numerical model. In this section, the main properties of the DHI TLP physical model, comparison of the main features with the reference structure (MIT/NREL TLP), and test information are given.

2.1. DHI TLP physical model and instrumentation

DHI TLP is a 1:40 Froude scaled model of the MIT/NREL TLP standard design (fig. 1(a) (Matha, 2010)). The main features of MIT/NREL TLP, DHI TLP numerical, and physical models are listed in table 1. Dimensions of the DHI TLP physical model are given in both model (scaled) and full-scale dimensions. The floater model was constructed out of plastic material (fig. 1(b)). Four mooring lines connected the structure to the basin base. A steel plate connected the four mooring legs (spokes, pontoons) to the structure. The serial connection of mooring rope, load cell, and spring ended up with an axial stiffness of 14.7 MN/m. It should be noted that the reference value is 20 MN/m (Matha, 2010).

The tower was designed rigid, constructed from plastic material, and was mounted on top of a TLP tank cover, which was 30 cm long and 16 cm in diameter (model scale). Mean still water level coincides with the top of the main cylinder. Tower rotor blades were geometrically scaled and constructed from fiberglass material (Armenio and D'Alessandro, 2013). An electric motor was placed inside the nacelle, which rotated the rotor at rated wind speed. In order to reach the reference thrust force at rated wind speed, an additional horizontal force was applied at the nacelle level by means of a pulley.

Table 1
Principal features

Feature	Unit	MIT/NREL TLP	DHI TLP-PHY(full/scaled)	DHI TLP-NUM
Platform radius	m	9.0	9.0/0.225	9.0
Platform height	m	47.89	47.89/1.1973	47.89
Pontoon length	m	18.0	18.0/0.45	18.0
CM location	m	40.61	40.61/1.0153	40.61
Tower height	m	90	90/2.25	90
Tower mass	kgs	347460	347500/5.2973	347460
Platform mass	kgs	8.6E6	8.6E6/131.0976	9022300
Total mass	kgs	9297500	9297500/141.7302	9806000
Water displacement	m^3	12187	12179/0.1903	12696
Unstretched line length	m	151.73	151.7/3.7925	151.58

Scaled model tests were conducted at the Offshore Wave Basin of Danish Hydraulic Institute (DHI) in Hørsholm, Denmark (fig. 1(b)), which is 20 m in width and 30 m in length. The wave maker is composed of 60 individually controllable wave flaps with a paddle length of 1.5 m capable of producing multi-directional wave spectra. A 6-DoF (Degree of Freedom) marine track system followed the rigid body motion of the platform. Five passive spherical markers, 40 mm in diameter, reflected the infrared light and were placed on a frame that was mounted at the tower base (Armenio and D'Alessandro (2013)). Gravity and shear forces, bending moment, and torsional moment at the tower base were captured by a 6-way force gauge that was located between the tower and the TLP cover. The gauge was 14 cm long (personal communication with DHI). Similarly, shear and bending moments under the Rotor Nacelle Assembly (RNA) were measured by using a 4-way force gauge. Accelerometers were attached to the tower base and under the nacelle. S-type load cells were attached between the springs and mooring lines to monitor the tension in the mooring lines. Wave kinematics were measured during the tests by using 11 wave gauges. Wave Gauge (WG) layout is given in figure 1(c).

Six WGs were placed around the model, and a WG array that consists of five WGs was placed ahead of the model. It should be noted that the distance between the WG array and WGs 1-3 is 40 m, which is 20 m less than the value given by Armenio and D'Alessandro (2013). The motivation for this correction was raised due to the delay detected during the estimation of wave elevation time series measured by WG5 by using a WG inside the WG array. Details of the procedure to estimate the wave elevation time series are given in the next section. With the layout given in figure 1(c), the estimations resulted without any delay. As shown in the next section, WG measurements taken during the physical tests are used as wave elevation input in time-domain analyses. WG1 to WG6 is not preferred due to possible radiated waves from the turbine model. For this purpose, WG9 measurements are used due to the closest estimations of WG5 measurements and constant variance values from the same irregular wave cases with different takes.

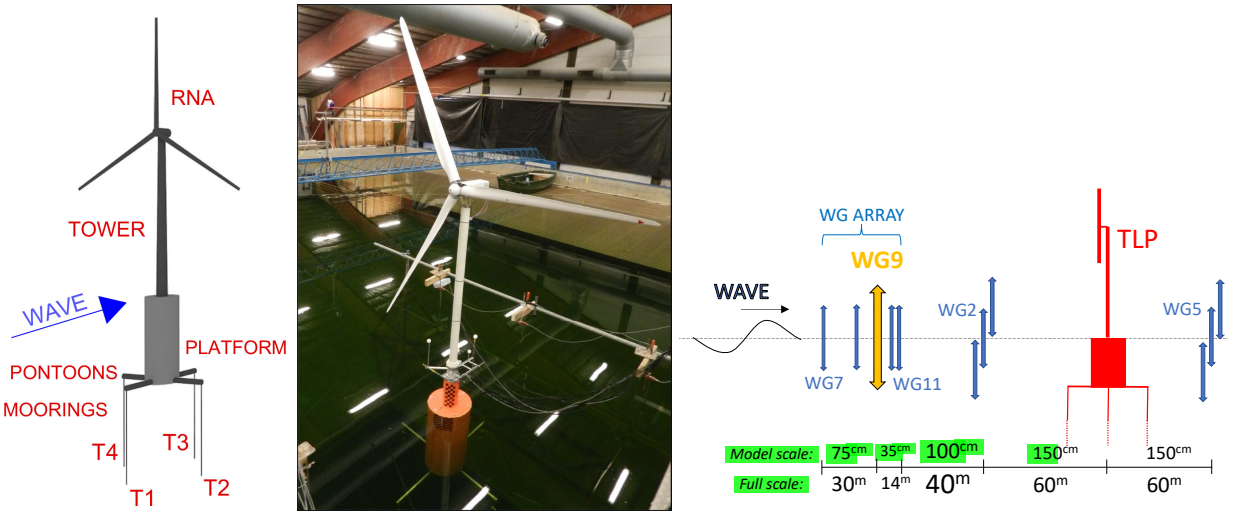

(a) MIT/NREL TLP wind turbine (b) DHI TLP physical model. Source: Armenio and D'Alessandro (2013) (c) Wave gauge layout. Edited from: Armenio and D'Alessandro (2013)

Figure 1: DHI TLP model

2.2. Test information

Static and free decay tests were conducted with/out tension in the mooring lines. Regular and irregular wave tests were conducted with/out mean static wind loading. Information on the decay tests, wave type, target value, and real (measured) values of wave height and wave period are given in Table 2.

Table 2
Physical test matrix.

Test #	type	direction	information		
T1207	DECAY	Heave	with tower, no tendons		
T1271	DECAY	Sway	with tower and tendons		
T1332	DECAY	Tower	with tower and tendons		
Test #	**Wave type**	$H_{target}(m)$	$T_{target}(s)$	$H_{real}(m)$	$T_{real}(s)$
T1274	REG	1.00	10.1	1.04	10.1
T1278	REG	4.00	11.4	3.46	11.4
T1279	REG	6.00	11.4	5.40	11.4
T1280	REG	8.00	11.4	7.10	11.4
T1275	REG	1.60	12.7	1.40	12.6
T1281	REG	6.00	12.7	6.22	12.7
T1277	REG	1.80	15.2	1.60	15.3
T1282	REG	6.00	15.2	6.36	15.2
Test #	**Wave type**	$Hs_{target}(m)$	$Tp_{target}(s)$	$Hs_{real}(m)$	$Tp_{real}(s)$
T1283	IRR	4.00	10.1	4.00	10.1
T1284	IRR	4.00	10.1	4.00	10.1
T1321	IRR	4.00	10.1	4.00	10.1
T1322	IRR	6.00	10.1	6.00	10.1

In physical tests with wind excitation, wind loading on the turbine was simplified by considering only a static wind loading without any turbulent effect. Consequently, a corresponding validation of turbulent wind effects can't be performed by comparing the numerical results against the test results.

3. Numerical modeling

In this study, numerical evaluation of a FWT is accomplished in two main steps: Frequency-domain preprocess and time-domain analyses. Frequency domain preprocessing is relatively simpler than time-domain analysis in terms of calculation efforts. In particular, Chakrabarti (1987) states that frequency domain analysis is useful for long-term response predictions or at the preliminary design stage. On the other hand, time-domain analysis allows for the consideration of nonlinear loads (Bachynski (2014)).

In the scope of this work, numerical analyses are conducted on the MIT/NREL TLP wind turbine, considering the properties of a scaled experimental model. Numerical analyses have been carried out in full-scale dimensions. TLP has three translational and three rotational degrees of freedom. Water depth is considered as 200 m, the reference value (Matha, 2010). Geometrical properties, mass, and stiffness of the platform and the turbine are summarized in Section 2. Detailed information is given by Vardaroglu et al. (2020), Armenio and D'Alessandro (2013).

Wave excitation forces and hydrodynamic coefficients that depend on the floater geometry are calculated in the frequency domain by using the open-source tool NEMOH (Babarit and Delhommeau, 2015). Calculated values for each wave frequency are used in time-domain analyses of the parked turbine, where the floater is subjected to orthogonal waves. For this purpose, the open-source code, *aero-hydro-servo-elastic coupled simulation tool: OpenFAST* (NREL) is used. In this section, each tool is briefly introduced, the interaction of each numerical tool with each other is explained. As a brief guide, figure 2 visualizes the whole numerical procedure in a flow chart.

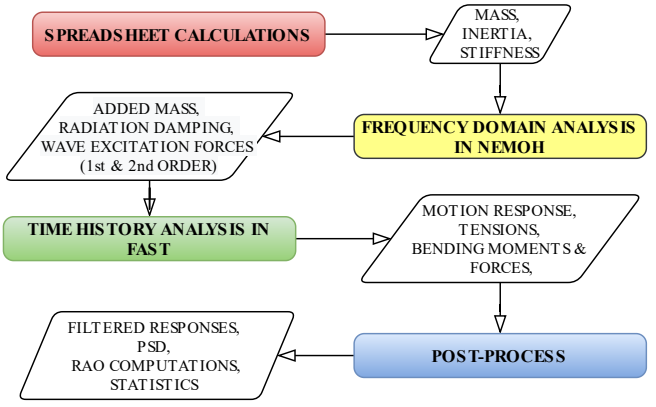

Figure 2: Computational sequence

A simplified numerical model has already been introduced by Vardaroglu et al. (2020); where hydrodynamic coefficients, first-order wave loads, tower mode shape coefficients were adopted directly from readily available values calculated by NREL. In this paper, hydrodynamic coefficients, first-order wave excitation loads, mean-drift wave loads are computed in the frequency domain, where pontoons are also considered. Superstructure (tower and the rotor) dynamics depend on the stiffness of the tendons, which act as a flexible structural foundation. Accordingly, tower bending mode shapes the calculated and updated in the time domain by using BModes (Bir, 2005), taking into account the tendon stiffness of the scaled model tested in the wave basin (DHI TLP physical model).

3.1. Hydrodynamic theory and modeling

A FWT can be modeled as a 6 DoF rigid body that can be analyzed as a mass-spring & damper system. Equation of motion in the frequency domain considering regular waves and induced loads and responses is written as follows:

$$[\overline{\overline{M}} + \overline{\overline{A}}(\omega)]\ddot{\overline{\eta}}(\omega) + [\overline{\overline{B_1}} + \overline{\overline{B}}(\omega)]\dot{\overline{\eta}}(\omega) + [\overline{\overline{C}}_{Hst} + \overline{\overline{C}}_{Line}]\overline{\eta}(\omega) = \overline{F}(\omega) \tag{1}$$

where:

- *Mass matrix*: Combination of the structural mass matrix ($\overline{\overline{M}}$), added mass matrix ($\overline{\overline{A}}(\omega)$) due to the outgoing radiated waves created by the floater motion

- *Linear damping matrix*: Potential damping due to the radiated waves around the platform ($\overline{\overline{B}}(\omega)$) and linearized viscous damping matrix ($\overline{\overline{B_1}}$)
- *Linear stiffness matrix*: Due to linear hydrostatics ($\overline{\overline{C}}_{Hst}$) and moorings ($\overline{\overline{C}}_{Line}$)
- $\overline{\eta}(\omega)$ is the motion response vector and $\overline{F}(\omega)$ is the wave excitation force vector.

Faltinsen (1993) handles the hydrodynamic problem -assuming linearity under steady-state (the weight of the body is equal to the weight of the displaced water in the mean position) conditions- in two-sub problems: *Diffraction problem:* There are incident waves, but the structure is restrained from oscillating. *Radiation problem*: The structure is forced to oscillate with the wave excitation frequency to satisfy the impermeability condition oppositely with respect to the incident waves. These problems are based on the calculation of fluid pressure on the wet surfaces of the structure, which can be obtained by solving the velocity potential, a Boundary Value Problem (BVP). Governing equation for the solution of the velocity potential is the Laplace equation: $\nabla^2\phi = 0$, where $\phi = \phi_1\varepsilon + \phi_2\varepsilon^2 + \phi_3\varepsilon^3 + ...$ The resulting velocity potential not only includes the linear part but also allows considering the nonlinearities (ε) in the free-surface waves and the motions (Greco (2012)). Once the velocity potential is obtained, pressure around the wet surface can be calculated. Forces and moments are obtained by integrating the pressure along the submerged surfaces. Linear wave loads on the structure can be obtained by ignoring the nonlinear term in Bernoulli Equation. Integration of the dynamic pressure over the wet surfaces accounts for the total linear wave loading on the FWT in 6 DoF. Moreover, considering linearity, two sub-problems (diffraction and radiation problems) can be superimposed. Accordingly, velocity potential can be separated into two subparts: Diffraction and radiation potential.

Solution of the radiation problem gives the added mass and damping terms A, B in Equation 1 for the related degrees of freedom. Solution of the diffraction problem leads to Froude-Krylov loads and diffraction (scattering) loads. The summation of these forces results in the total wave excitation forces on the floating wind turbine platform. When loading is limited to wave effects, Faltinsen (1993) suggests a frequency-domain approach, where nonlinear contributions to the wave excitation load are excluded, and the wave excitation can be assumed as harmonic;

$$\overline{F}_{exc,j}(t) = \zeta \Re \left\{ e^{i\omega t} \overline{X}_j(\omega, \beta) \right\} \tag{2}$$

where $X_j(\omega,\beta)$ is the transfer function for the excitation loads for the jth wave with frequency (ω) and head angle (β). The resulting force is proportional to the wave amplitude, ζ and oscillates harmonically with wave frequency ω. First-order potential theory serves to calculate linear wave loads on offshore structures and FWTs. Velocity potential first-order terms are used for the purpose, $\varepsilon = k\zeta$, where k is the wavenumber. As the wave steepness increases with the increasing wave amplitude, higher-order elements in the velocity potential, e.g., ε^2 need to be considered. Even though the contribution of second-order wave effects is relatively small compared to the linear wave loads, computation of second-order wave forces requires the consideration of a wide range of frequencies from the wave spectrum. Considering ω_i and ω_j from the wave spectrum, the interaction between two wave frequencies will result in second-order wave loads on the structure. Faltinsen (1993) states that the difference between two very similar frequencies generates slowly-varying excitation forces and moments that may cause resonance oscillations in the surge, sway, and yaw motions in moored structures. For a TLP FWT, the natural periods of platform heave, pitch, and roll are designed so that the natural periods are smaller than those of the wave periods to avoid resonance. Accordingly, second-order sum-frequency wave loads will excite these resonant motions and should be considered.

Equations 1 & 2 shows that the solution is dependent on the incident wave frequency. Accordingly, the problem is handled in frequency-domain, and added mass coefficients, radiation damping coefficients, wave excitation force is obtained for each wave frequency. A BVP can be solved numerically according to Boundary Element Method (BEM), which is also known as *panel method*. In this study, an open-source BEM solver, NEMOH (Babarit and Delhommeau, 2015) is used, which is a diffraction/radiation linear potential flow solver and calculates the wave part of Green's function using interpolation and solves the flow problem using source distribution technique (Babarit and Delhommeau, 2015),(Penalba, Kelly and Ringwood, 2017). Only the wet surfaces are considered. Accordingly, only the main cylinder and the pontoons are modeled. Panels can be in quadrilateral or triangular shapes. In this study, mesh generation is handled by external software, a 3-D finite element mesh generator, *GMSH* (Geuzaine and Remacle, 2009). A Python module, *Meshmagick* (Buisson and Rongére, 2017) is used to convert the GMSH output to the

necessary mesh input needed for hydrodynamic analysis. Veritas (2010a) advises the diagonal length of a panel to be smaller than 1/6 of the smallest wavelength analyzed. Considering that the smallest wave period is 3.14 sec (2π rad/s), the corresponding maximum diagonal size can be 2.60 m. Accordingly, the base mesh is generated with equilateral triangular elements with a 1 m side length. Sidewall mesh is generated with quadrilateral elements in 1.50 m length. Part of the mesh is shown in Fig. 3(a) and Fig. 3(b). NEMOH allows symmetry only around one plane. Since the MIT/NREL TLP platform is axisymmetrical, symmetry around the x-x axis is used, and half of the platform, including the pontoons is modeled. Pontoons are represented with triangular and quadrilateral elements with 1m of side length. In the figures, arrows show the surface normals, which should point outwards. In summary, the generated mesh has 1577 nodes and 1642 panels (426 triangular elements, 1216 quadrilateral elements).

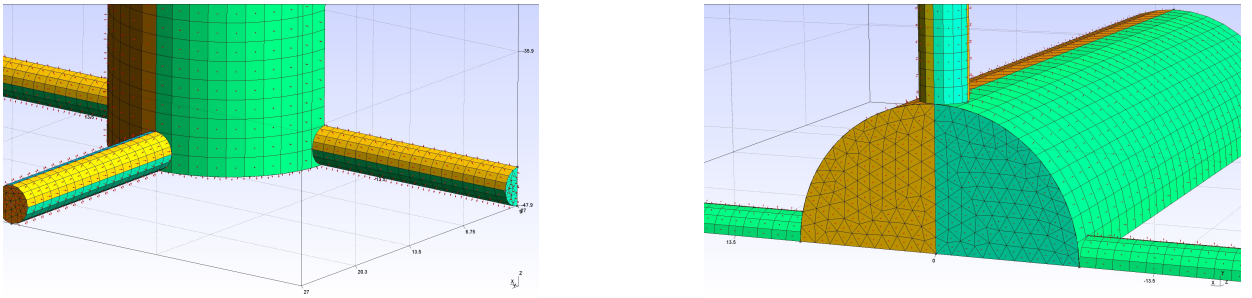

(a) back-side view

(b) bottom view

Figure 3: Mesh for frequency domain analyses

Frequency-domain computations are executed with a frequency resolution of 0.05 Hz. Mass, inertia, and stiffness values of the system are calculated with spreadsheets. Added mass, hydrostatic stiffness, and mooring stiffness equations are readily available in the literature (Bachynski, 2014). Mooring stiffness values are computed based on the mooring line stiffness of the wave basin model. Calculated mooring stiffness is cross-checked with the Python wrapper *Static Configuration* for MAP++ by Masciola (2015). The resulting mass and the total stiffness (hydrostatic+mooring stiffness) values are:

$$diag[M] = \begin{bmatrix} 9.81E6 & 9.81E6 & 9.81E6 & 1.91E10 & 1.91E10 & 6.24E08 \end{bmatrix} (kg; kg \cdot m)$$

$$(K_T) = \begin{bmatrix} 2.14E5 & 0 & 0 & 0 & -9.93E6 & 0 \\ 0 & 2.14E5 & 0 & 9.93E6 & 0 & 0 \\ 0 & 0 & 5.91E7 & 0 & 0 & 0 \\ - & - & - & 2.20E10 & 0 & 0 \\ - & - & SYM & - & 2.20E10 & 0 \\ - & - & - & - & - & 1.56E8 \end{bmatrix} (N/m; N; N \cdot m/rad; N/rad)$$

NEMOH computes mean-drift loads on the wet surfaces according to the far-field formula (a.k.a momentum conservation method) upon the calculation of first-order outputs (Philippe, Combourieu, Peyrard, Robaux, Delhommeau and Babarit, 2015). For this purpose, Kochin functions are calculated for each BVP. For each wave frequency, it is possible to have a maximum of seven BVP (one diffraction & six radiation). The far-field formulation is restricted to calculate only the horizontal components (surge, sway, and yaw) of the mean-drift wave force (Thomsen, 2017). Each Kochin function is calculated by using Response Amplitude Operator (RAO) values from the linear solution and consists of a part associated with the diffraction potential, corresponding radiation potential (Arnal, 2016).

Results of the hydrodynamic analysis are compared with the reference values calculated on MIT/NREL TLP by Matha (2010). Consideration of the pontoons in the frequency-domain resulted with +6.1%, +45%, +16.6% and +1.0%, -11.0%, +7.2% maximum differences with respect to the reference added mass and radiation damping coefficients in the surge, heave and pitch directions. Moreover, a 134% increase in the projected area in the vertical direction

results in a 45% increment in the added mass, but -11% decrease in the radiation damping coefficients. Moreover, +1.3%, 0.0%, +5.9% difference in the first-order wave excitation forces in the surge, heave, and pitch directions show that the linear wave forces are slightly affected from the presence of the pontoons located at -49.39 meters depth.

3.2. Motion response analysis

In this study, motion response analyses are conducted in the time-domain under regular & irregular orthogonal waves. Natural periods and damping ratios are calculated from free decay analyses. Results are compared with the wave basin test results in the following sections. Cases including wind excitation are not in the scope of this paper due to the relatively simplified wind loading on the scaled physical model (see Section 2). Figure 4 shows the organization of the time-domain analysis routine with the modules and the necessary inputs. HydroDyn ()Jonkman, Robertson and Hayman, 2014 (accessed October 16, 2020) is used to solve the Hydrodynamics problem; MoorDyn (Hall, 2015) is for dynamic mooring line solutions. AeroDyn (Moriarty and Hansen, 2005) deals with the aerodynamics problem but is not a part of the solution in this study. ElastoDyn includes structural models of the rotor nacelle assembly, tower, and the platform (Jonkman, 2013).

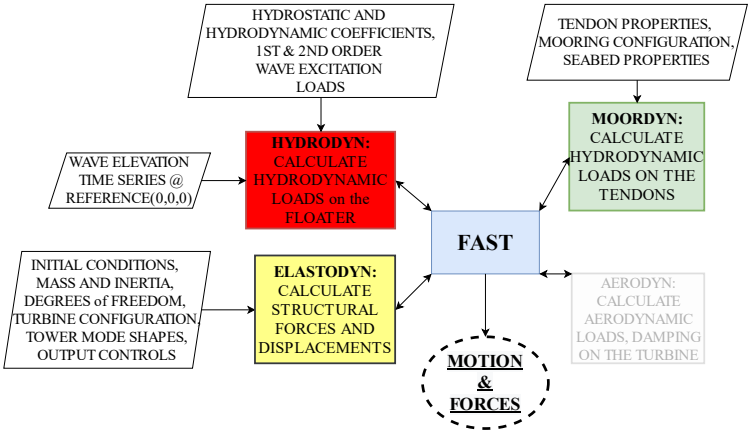

Figure 4: Motion response analysis scheme

The precision of the time-domain analyses is increased by using WG measurements such as wave elevation time series in HydroDyn. Input location is only available at the origin of the coordinate system, where the TLP wind turbine is placed. In this study, WG9 (fig. 1(c)) data is used for the regular and irregular wave analyses. For this purpose, wave gauge measurements are decomposed into harmonical components with amplitudes and phases using Fast Fourier Transforms (FFT). Following that, wave elevation time series at turbine location is estimated by using:

$$\zeta(x,t) = \sum_{j=1}^{N} \zeta_j \cos(\omega_j t - (\frac{2\pi}{\lambda_j})x + \varepsilon_j) \tag{3}$$

where, $\zeta(x,t)$ is the wave elevation time series. ζ_j is the amplitude of the jth regular wave in the time-domain that is equal to $\sqrt{S(\omega_j)\Delta\omega}$, where $S(\omega_j)$ is the wave spectrum and $\Delta\omega$ is the wave frequency step in the spectrum discretization. λ_j is the wavelength, $2\pi/\lambda_j$ is the wavenumber k_j, ε_j is the random phase of jth regular wave component, x is the distance between the turbine and the corresponding WG.

HydroDyn module is responsible for the calculation of the hydrodynamic loads on the platform in the time-domain, using the linear theory (Jonkman, 2007). According to the assumption of linearized-hydrodynamics, the amplitude of an incident wave is smaller than the wavelength. Consequently, the Airy wave theory is valid. Translational displacements of the support platform are small relative to the size of the body. It permits the hydrodynamic problem to split into three problems: Radiation, Diffraction, and Hydrostatics. As a result of linearization, superposition principles can be applied (Jonkman, 2007). Accordingly, total excitation load on the support platform from first-order incident

waves can be expressed such as;

$$(\overline{\overline{M}} + \overline{\overline{A}})\ddot{\overline{\eta}} + \int_0^t \overline{\overline{K}}(t-\tau)\dot{\overline{\eta}}(t)(\tau)d\tau + (\overline{\overline{C}}_{Hst} + \overline{\overline{C}}_{Line})\overline{\eta} = \overline{F}(t) \tag{4}$$

where $\overline{\eta}$ is the motion response vector in six DoF. The first term in the Equation 4 is the inertia component. Equation of motion in the frequency domain (eqn. 1) is transformed into the nonlinear time-domain analyses by using Cummins equation, which adds an impulse-response function, a Duhamel integral, called the retardation function (Kvittem, 2014). The retardation function is represented with $\overline{\overline{K}}$, within the second term in Equation 4. The retardation function accounts for frequency-dependent added mass and linear radiation damping in the time domain. The final term is the restoring component, which is the sum of hydrostatic and mooring stiffness.

Nonlinear viscous-drag loads are computed in HydroDyn by using Morison's representation in conjunction with strip theory. In hydrodynamic strip theory, the structure is split into several elements or strips, where two-dimensional properties, such as added-mass and viscous-drag coefficients are used to determine the overall three-dimensional loading on the structure (Jonkman, 2007). Jonkman (2007) expresses the total external load acting on the platform for surge and sway modes of motion (i=1,2) according to Morison's representation by integrating the load on each strip:

$$dF_i^{Platform}(t,x,y,z) = -\rho C_A(\frac{\pi D^2}{4}dz)\ddot{x}_i(t,x,y,z) + \rho(1+C_A)(\frac{\pi D^2}{4}dz)a_i(t,x,y,z) + \frac{1}{2}\rho C_D(Ddz)[v_i(t,0,0,z) - \dot{x}_i(z)]\left|v_i(t,x,y,z) - \dot{x}_i(z)\right| \tag{5}$$

where,

- i represents the ith strip
- ρ is seawater density, D is the diameter of the platform, and dz is the infinitesimal length of the strip of the platform
- C_A & C_D are non-dimensional hydrodynamic added mass and viscous drag coefficients
- v_i & a_i are the undisturbed wave particle velocity and acceleration on the ith strip of the floater.
- The last two terms constitute $dF_i^{Viscous}$, which is the viscous-drag load acting on the strip of each cylinder. x represents the motion of a strip. The term $\pi\ D^2$ dz/4 is the displaced volume of fluid for the strip of the cylinder. $D \cdot dz$ is the projected area of the cylinder.

HydroDyn presents multiple approaches for calculating the hydrodynamic loads (Jonkman et al., 2014 (accessed October 16, 2020). In this study, a hybrid approach in which the potential-flow solution is combined with strip theory solutions is chosen to consider the viscous damping effects. In the potential flow theory solution, added mass, diffraction, Froude – Krylov, and radiation damping wave loads are calculated on the wet surfaces of the structure. The resulting added mass & radiation damping coefficients are used in motion response analysis. For the strip theory approach, the platform is divided into 100 strips in the vertical direction. Pontoons are divided into strips of 0.50 m in length. Viscous drag coefficients in transverse direction -in the same direction as the resulting velocity-, C_d for the platform and the pontoons are calculated as 0.7 considering the circular cross-sections according to Veritas (2010b). It should be noted that the added mass coefficient, C_a, is not considered in the strip theory solution since it has already been accounted for in the potential flow theory calculations.

HydroDyn allows the computation of second-order wave excitation forces by using the first-order wave amplitudes and adds extra energy to the wave spectrum at the difference and sum frequencies. Jonkman et al. (2014 (accessed October 16, 2020) reports that once the second-order wave forces are considered, some of the nonlinearities of the real surface waves can be captured. This allows more accurate modeling of sea states and corresponding wave forces (Jonkman et al., 2014 (accessed October 16, 2020). HydroDyn can be operated in three ways to consider second-order wave loads: only the mean-drift loads can be calculated, or mean and slow-drift terms can be estimated by using

Standing et al's extension (Standing, Brendling and Wilson, 1987) to Newman's approximation, or mean and slow-drift terms can be calculated by using the full difference-frequency Quadratic transfer function (QTF). In this study, mean and slow-drift terms are estimated by using Standing et al's extension to Newman's approximation. Mean-drift loads are calculated during the frequency-domain analysis whilst considering the horizontal degrees of freedom (surge, sway, and yaw) according to the momentum-conservation method.

In summary, motion response analyses in the time-domain are conducted by considering the first-order wave loads in six platform DoF and the second-order difference frequency wave loads for surge and sway DoFs using Newman's Approximation. Second-order difference frequency loads are not taken into account in heave, pitch, and roll DoF, which are not important for TLP. Due to wave orthogonality, yaw moments and motion are small and neglected.

FAST allows quasi-static or dynamic solutions for mooring line computations. MoorDyn (Hall, 2015) is based on the lumped-mass approach and considers the mooring stiffness, inertia, weight, buoyancy, and friction between the mooring cable and the seabed. In addition to the quasi-static module MAP++ (Masciola, 2016), MoorDyn considers line damping and the viscous drag forces on the line and is chosen for this study. Four pairs of lines are placed at each fairlead location, wherein a total of 8 lines are defined. The unstretched line length is 151.58m. Equivalent mooring line extensional stiffness, EA, the product of elasticity modulus and cross-sectional area is 1120 MN. Each line is divided into 20 mass-spring-damper elements (Maxwell links). Line internal damping ratio is set to 95% of the critical damping to avoid the artificial resonance that can be created by the discretization. On the other hand, in order to take into account the damping effects, viscous drag coefficient in the transverse direction, C_{dn} is considered as 1.0 and added mass coefficient, C_{an}, is chosen as 1.0 considering the circular cross-sections according to (Veritas, 2010b).

The superstructure (tower and the RNA) is linked to the motion response analysis via the ElastoDyn module. NREL 5-MW reference turbine mass, stiffness, and inertia values are obtained from Jonkman, Butterfield, Musial and Scott (2009). The tower is modeled with 21 nodes and 20 Bernoulli-Euler beams considering only the bending deformations. In other words, shear deformations, axial and torsional displacements are neglected. Small to moderate deflections are considered, where mode shapes are used as shape functions in a nonlinear beam model (Rayleigh-Ritz method). It should be noted that ElastoDyn does not compute mode shapes internally (Jonkman, 2013). BModes is used for this purpose by considering the mass, inertia, and stiffness of the tower, platform, and RNA. In the case of a TLP wind turbine, tensioned tendons act like a flexible foundation and affect the superstructure dynamic behavior. BModes computes the deflection along with the tower height. Followingly, polynomial coefficients are calculated from the deflection data.

3.3. Calibration of the numerical model

HydroDyn allows the application of additional preloading, stiffness, and damping to the time-domain analysis model. This gives the chance to tune the numerical model characteristics (e.g., natural periods, damping ratios) according to the experimental model. In this study, the damping ratio of the numerical model is tuned according to a sway free decay test. A comparison of the numerical and the experimental models is given in Table 3.

Table 3
Properties of the numerical model and of the physical model.

	Numerical Model	Test Model
Floater	Rigid	Rigid
Tendons	Lumped mass multi-DoF model	Spring + force gauge + rope
Tower	Flexible	Rigid
Rotor	Flexible & parked	Rigid & parked

According to Armenio and D'Alessandro (2013), decay tests on the tensioned scaled model were conducted only in the sway direction, where the physical model was displaced 7.9 m -full-scale value- in positive sway direction with the accompanying 20 cm in heave due to the set-down effect for the TLP. Heave set-off is cross-checked with a simple hand calculation, neglecting the elongation in the tendons. Test duration was 360 s in full scale. Free decay analysis was conducted by applying an initial sway and heave displacements to the numerical model at rest and then releasing the structure to oscillate. The time step is constant at 0.01 s. In this paper, the calibration process given by Vardaroglu et al. (2020) is repeated with the updated numerical model.

Viscous drag forces on the platform in the transverse direction are already considered in the computations with the

viscous drag coefficient, C_d. Additional linear damping controls in HydroDyn are utilized to tune the damping in the numerical model according to the physical model. Additional linear damping is accounted for the viscous drag on the platform in surge and sway directions and the structural damping in heave direction due to the vibration of the tendons, which is not considered in the MoorDyn. Accordingly, additional linear damping is defined to adjust the damping in the surge, sway, heave, roll and pitch DoFs. In conclusion, an additional 2.5% of the critical damping in sway (and surge), 1% of the critical damping in heave, 1% of the critical damping in platform roll (also pitch) is added as linear damping to the system. Critical damping simply implies to the ratio of the damping constant c to the critical damping constant c_{cr} of a viscously damped free vibrating system (Chopra, 2007), $2m\omega_n$ or $2\sqrt{km}$, where k is the total stiffness, m is the total mass of the system, including the added mass value at the natural frequency of the corresponding DoF. Results of the analyses are listed in Table 4, which also compares the results of the physical decay test. The resulting natural period and damping values are computed from the peaks of the time-history plots. The damping ratio is calculated according to the logarithmic decrement method. Due to the lack of physical decay tests in heave, pitch DoFs, damping in heave, and pitch are tuned from the sway decay test. Since the responses are coupled to each other, time histories of the responses are filtered around the relevant natural frequency. Band-pass filters are used for this purpose. Necessary frequency intervals are obtained from spectral density plots (PSD). It should be noted that the resulting data from free decay analysis is non-stationary data. Spectral analysis on non-stationary data is not a healthy process. Accordingly, PSD plots are only used to detect frequency intervals for filtering. Although only surge (sway) and heave DoF are visible in Table 4, due to the symmetry, surge & sway and roll & pitch natural periods and damping ratio should be very close.

Table 4
Comparison of the natural periods and damping ratios of the numerical and physical model

	Period(s)			Damping ratio(%)		
	Numerical	Physical	Diff(%)	Numerical	Physical	Diff(%)
surge	68.0	56.3	20.8	4.9	5.0	-2.0
pitch	5.0	5.5	-8.9	3.7	3.9	-5.1
heave	2.7	2.9	-6.5	1.2	1.0	20
Tower FA 1st mode	1.7	2.0	-17.8	3.6	3.1	16.1

According to Table 4, the natural period of the numerical model in heave is 2.7 s. This value cross-checks with the hand calculations, in which the added mass value is evaluated at the natural heave period. The corresponding value for the physical test is 2.9 s (8% higher), which is directly linked to the scaled model tendon stiffness. Similarly, platform pitch natural (the coupled platform pitch and tower fore-aft bending first mode, where platform pitch dominates the mode shape) period also results in 9% of difference. It should be reminded that the geometry, mass, stiffness, and the initial conditions of the numerical model are arranged according to the data obtained from the test reports (Armenio and D'Alessandro (2013), Armenio (2014), Tomasicchio et al. (2014)). Furthermore, the natural period of the updated numerical model in surge is 4 s larger than the value indicated by (Vardaroglu et al., 2020) value. It can be explained by the increased added mass of the updated numerical model with the presence of the pontoons. On the other hand, the natural period of the DHI TLP numerical model in the surge (also sway) is calculated 21% higher than the DHI TLP experimental model. The percentage implies the ratio of the difference between the two results divided by the experimental result. The reference value for the sway period is 60.6 s (Matha, 2010), where the pontoons are not considered in the frequency-domain model, and the total axial tendon stiffness value is 34% larger than the DHI TLP experimental model value. Vardaroglu et al. (2020) also reported that the un-tensioned heave natural period measurement from physical test T1207 is 12.9 s., which cross-checks with the hand calculation for MIT/NREL TLP, where pontoons were not considered. In the case of DHI TLP, the natural period in heave is calculated as 13.7 s. The difference is related to the presence of the pontoons, which resulted in an increase in ballast mass and added mass.

In summary, it is understood that the DHI TLP physical model is more stiff compared to the reference MIT/NREL TLP (Matha, 2010) in the surge (also sway) but with relatively loose tendons. At this point, Vardaroglu et al. (2020) points out possible uncertainties in the wave basin test setup, which can be accounted for simply an offset of the acquisition system or possible error sources in the model design and numerical modeling. In conclusion, the authors have an impression that the sensor cables attached to the scaled TLP model in the experimental study might have altered the structural characteristics such as the stiffness and mass distribution, which may source the difference in the

natural periods.

In addition to the findings from sway decay test, "free decay tower test" data is also investigated, which was conducted with tensioned lines, parked rotor, and the tower was mounted to the platform. Spectral analysis of the tower base moment fore-aft bending moment response resulted in a peak at 0.48 Hz, which cross-checks the value obtained from the pitch component of sway free decay test. It should be noted that the reference value for the MIT/NREL TLP in tower base fore-aft bending first mode (coupled platform pitch and tower bending first mode in the fore-aft direction, where the tower bending dominates the mode shape) is 0.6311 Hz (Matha, 2010). The related value is 0.606 Hz for the DHI TLP numerical model.

Vardaroglu et al. (2020) has also conducted a sensitivity study on the damping behavior of the numerical model. It has been reported that the different initial conditions did not affect the damping behavior.

4. Response under regular waves

The DHI TLP physical model was tested under orthogonal regular waves without wind excitation within a wave period of 10.1 s to 15.2 s. The experimental duration was kept constant 1132 s with 6.32 Hz of sampling frequency. The computational time step is 0.01581 s, which is 1/10 of the physical model sampling value. The rotor is in parked condition during the analyses (Table 3). The wave elevation time series obtained in the previous section are used as wave input into HydroDyn. In addition to these analyses, DHI TLP numerical model is analyzed under regular wave elevation time series generated by HydroDyn to observe the response within a larger wave interval, which is considered between 5 s to 20 s. Additional analyses between wave periods of 2.5 s and 5 s are also conducted, which is the natural period zone of the DHI TLP. Numerical analyses results of DHI TLP wind turbine under regular wave excitation are evaluated by using RAO since wind excitation, nonlinearities in wave input, structural nonlinearities are not considered in the analysis. For this purpose, amplitudes of each response and the actual wave height from each test are calculated by extracting the peaks of the related time histories between t=700 & t=1130 s. Test characteristics are listed in Table 2, where it is understood that the wave periods in the physical tests are in good agreement with the target values, where the resulting wave heights are changing - 6% to +13.5% with respect to the target values.

Figure 5(a) shows the RAO comparison of surge response from physical and numerical tests under regular waves. Data series in red and blue color represent the experimental and numerical analysis results on the DHI TLP. Data series in black color come from numerical analyses with unit wave height, which are aimed to add information on the whole incident regular wave interval. Figure 5(a) shows that both numerical and physical RAO values tend to increase with the increasing wave period. Due to the linearity in the numerical solution, RAOs from cases with different wave heights but the same wave period resulted in the same RAO value. It is not the case for the physical test response. Accordingly, a minimum 0.035 m/m, maximum 0.15 m/m difference is obtained between the numerical and physical model, which yields 7.2% and 33% larger responses in the numerical model compared to the physical model. According to the additional numerical analyses with unit wave height, a peak is visible at T=5.0 s, which corresponds to the pitch natural period. Heave RAOs are given in figure 5(b). The first observation from fig. 5(b) is the very low heave responses in both models, which is the expected behavior of a TLP due to the extremely large tendon stiffness. A peak that corresponds to the resonant response at heave natural period (2.7 s) is visible from unit-wave amplitude analyses. Adjacent peaks are also visible at exactly and between the heave and platform pitch natural modes. The differences between the physical and numerical models are accepted in logical limits due to the low heave magnitudes observed in both numerical and physical models.

Pitch RAO plot is given in figure 6(a). The vertical axis is in "deg/m". A peak at T=5.0 s with 1.04 deg/m is visible in Figure 6(a), which represents the platform pitch natural period. Following the peak, pitch RAOs tend to decrease for numerical and physical models with increasing wave periods. A close-up view of the numerical and physical response comparison with a vertical axis limit at 0.16 deg/m is also visible in fig. 6(a). Small differences are obtained between the numerical and physical models for all the experimented wave periods. Besides, at a wave period of 12.7 s, numerical analysis T1281 with a wave height of 6.0 m resulted in a 0.019 deg/m larger RAO value with respect to the physical case. The corresponding value for the numerical test (T1275), which has the same wave period but a wave height of 1.6 m resulted in 0.005 deg/m larger RAO compared to the physical test # 1275. A similar response is also observed at a wave period of 15.2 s. In summary, even though the numerical analyses resulted in larger RAO values, the differences are considered in acceptable limits due to the low responses observed in both numerical and physical models, which is the expected behavior from a TLP.

Figure 6(b) shows the tower base fore-aft direction moment comparison at 17.60 m above the still water level.

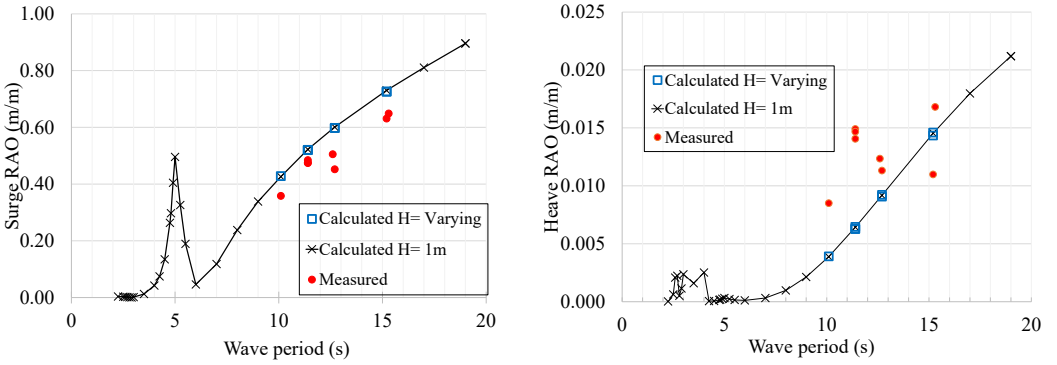

Figure 5: Regular wave RAO: Surge (left) and heave (right)

Accordingly, the resonant response at the platform pitch natural period is observed at the wave period of T=5.0 s from the unit wave height analysis. Additionally, the close-up view of numerical and physical model comparisons shows that the response increases up to the peak around 12 s for both models and then tends to decrease with the increasing wave period.

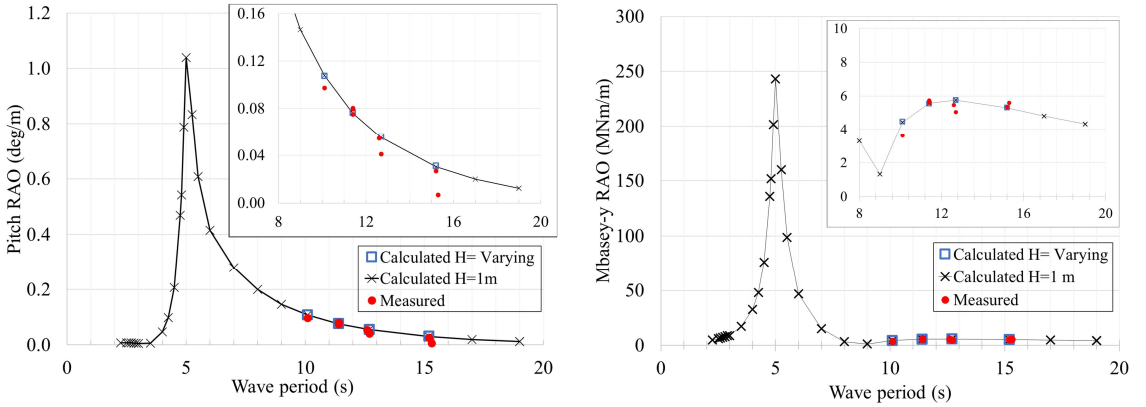

Figure 6: Regular wave RAO: Pitch (left), Tower base moment (right)

Figure 7(a) shows RAO comparisons of tension in line#1 (T1) and line#3 (T3). Tension line layout is given in figure 1(a). It is understood from figure 7(a) that T1 and T3 have a peak at pitch natural period, which is the expected response under wave excitation. Following that, the close-up view shows a closer look at the comparisons with physical test results. It is observed that the numerical model T1 and T3 responses are the same, which is the expected case under wave excitation from a TLP wind turbine. On the other hand, a visible reduction in T3 RAO is noticed in the physical model response for all the wave periods. In addition, the numerical model resulted in the same RAO values for different wave heights due to the linear solution. The physical model had similar differences as observed in fig. 6(a), where test T1282 with wave height, period of 6.0 meters, and 15.2 s resulted in an apparent off-trend value.

Side tension RAOs are compared in figure 7(b). T2 and T4 are governed by the platform surge and heave, and the variations are relatively small compared to T1 and T3. It is observed from figure 7(b) that the numerical model response for T2 and T4 are the same and increase with the increasing wave period. In the physical model, a similar response to the numerical model is noticed in some cases but with off-trend values. Physical RAO from T1282 has the same off-trend behavior that is observed in the other RAOs. Further investigation of the physical test T1282 data resulted in an in-phase yaw response in the time domain. In summary, the off-trend response of test T1282 is counted as an uncertainty in the physical tests. In summary, a good agreement is observed between the numerical model computation and physical model measurements.

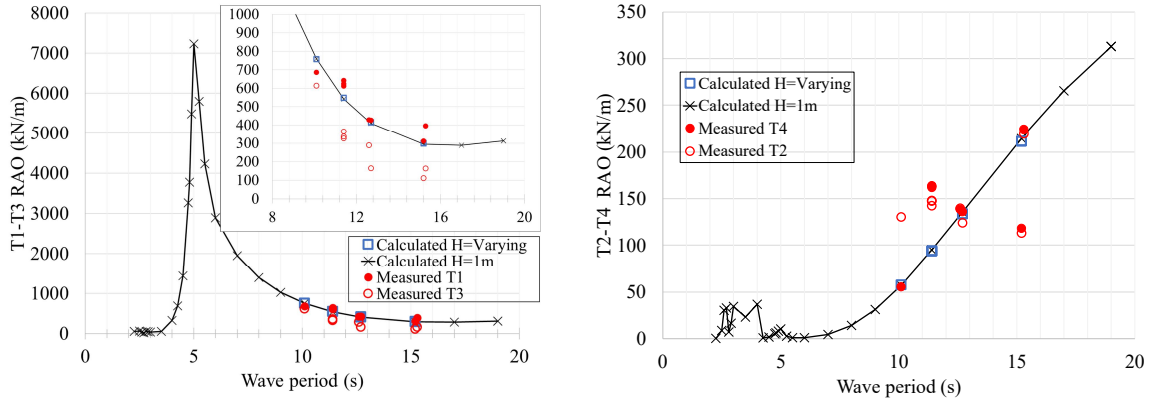

Figure 7: Regular wave RAO: T1-T3 (left), T2-T4 (right)

5. Response under irregular waves

In this section, the response of the DHI TLP physical and numerical model under irregular waves is presented and compared in terms of time histories, spectral densities, and statistics. In both models, the rotor is in parked condition, and incident waves are orthogonal to the TLP wind turbine. Armenio (2014) states that irregular waves were generated according to the JONSWAP spectrum with a peak-shape parameter value of 3.3. Table 2 shows that test T1283, T1284, and T1321 have the same wave characteristics. T1322 has the same peak wave period value but has six meters of significant wave height. Figure 8(a) shows spectral density plots of the measured irregular wave elevation time series from the offshore wave basin with variance values given in the legend. It is visible in figure 8(a) that T1283 and T1321 have the same wave spectrum shape and variance, but T1284 has a 10% larger area under the spectrum compared to T1283 and T1321, which accounts for a higher variance.

Numerical simulations are conducted by using wave gauge 9 (WG9) measurements taken during physical tests. It should be noted that the complete wave records are used in the numerical analyses, which are 3780 s long. On the other hand, the initial ten minutes (600 s) of each response is considered the transition phase and is not considered in the calculation of response statistics. Figure 8(b) shows a part of the measured wave elevation time series from test T1283 (black markers). Moreover, the measured time series is used to regenerate the time series (blue markers) at the gauge location by using FFT and IFFT. Finally, the estimated time series at the turbine location is given with the red line, which is 114 m away from the WG9. It is shown that the wave elevation time series are calculated with 100% precision at the gauge location.

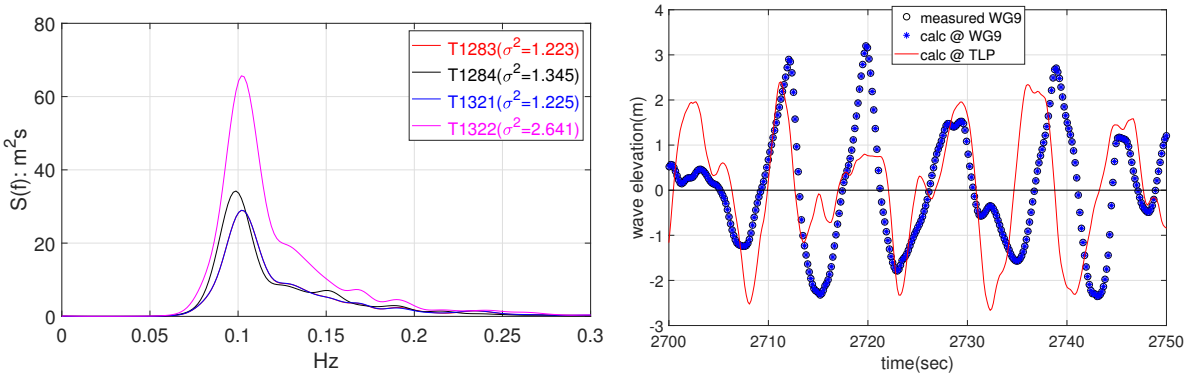

(a) Irregular wave spectrum from wave basin

(b) T1283 WG9 wave elevation measured vs calculated close-up view

Figure 8: Irregular wave kinematics

Physical and the numerical model response comparisons are given in the next figures. Spectral analyses are conducted by using the WAFO toolbox (Brodtkorb, Johannesson, Lindgren, Rychlik, Ryden, Sjö et al., 2000) and assessed for T1283 (four meters of peak wave height) and T1322 (six meters of wave height). T1322 with higher significant wave height yielded larger responses in all measured and calculated quantities. Responses in the time domain are extracted from T1283 and filtered for some cases.

Figure 9(a) shows a closer look at the zero-mean surge response in the time-domain from T1283, where the measured response is given with the red line and the calculated response from the numerical model is represented with the blue line. Figure 9(a) shows that both responses oscillate with the peak wave period (10.1 s) and surge natural frequency. Consideration of mean-drift forces in the numerical model resulted with the low-frequency component but with a phase shift due to the difference at surge natural frequency between the two models. Spectral analysis results are given in figure 9(b), where peaks are detected at surge natural frequencies (0.0147 and 0.0178 Hz), peak wave frequency -1X-(0.099 Hz), and pitch natural frequency (0.200 and 0.182 Hz) from the numerical and physical model. The area under each PSD plot is equal to the variance of the response. Corresponding values obtained from physical and numerical models are 0.55 and 0.37 m^2 for T1283, 1.21 and 1.17 m^2 for T1322. Accordingly, it is observed that consideration of the mean-drift loads in the numerical model resulted in close estimations of the physical model surge variances.

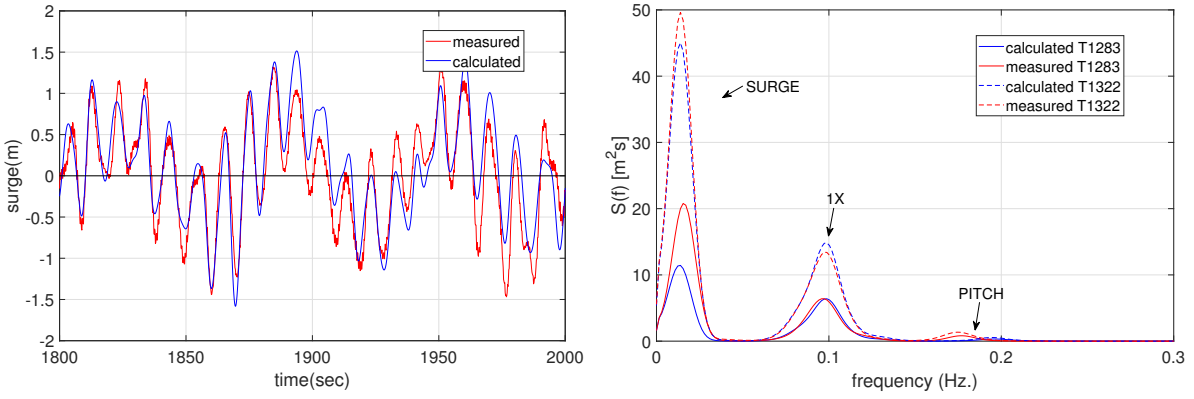

Figure 9: Surge response time history from T1283 (left) and PSD (right) comparison from T1283 and T1322

Figure 10 shows pitch response comparison. Spectral density plots are given for two different wave cases. Figure 10(a) shows that response is dominated by the coupled platform pitch and tower bending mode natural frequency, which is 0.18 Hz for the physical model and 0.20 Hz for the numerical model. Corresponding variances for the numerical and physical model are 0.078, 0.168 deg^2s and 0.152, 0.292 deg^2s for T1283 and T1322. Relatively small variance obtained with the numerical model can be explained by the different natural periods in pitch DoF, which affects the response amplitude (see fig. 6(a)). Peak spectral values are not evaluated here since the magnitudes can be affected by frequency resolution. The vertical axis is in degrees in fig. 10(b), where close magnitudes are accompanied by delays due to the different pitch natural frequencies of the physical and numerical model.

Tower fore-aft bending moment response is plotted in figure 11. Both responses from both tests are governed by the coupled pitch & tower fore-aft bending moment natural frequency around 0.2 Hz. Figure 11(a) indicates a weak peak at the peak wave frequency (0.1 Hz). In addition to that, another peak with a very low spectral density is observed around the tower fore-aft bending the first mode, which is 0.61 Hz for the numerical model and 0.5 Hz for the physical model. On the other hand, Tomasicchio et al. (2014) reports that the wind turbine model is rigid. Similar to figure 10(b), fig. 11(b) shows the tower base moment comparison in the time domain. Since the bending moment response is dominated by the coupled platform pitch mode, close values are obtained for both models but with a phase delay due to the difference in the pitch natural frequencies. Similar to fig. 10(a), the difference in the pitch natural periods between the two models resulted in different spectral shapes and variance values.

Tension in the first line (T1) responses are given in figure 12. The spectral plot in figure 12(a) is given for 4m and 6m wave height cases. Accordingly, T1 is composed of components at peak wave frequency, platform heave natural frequency, and platform pitch frequency that dominates the response. Platform heave natural frequency component is

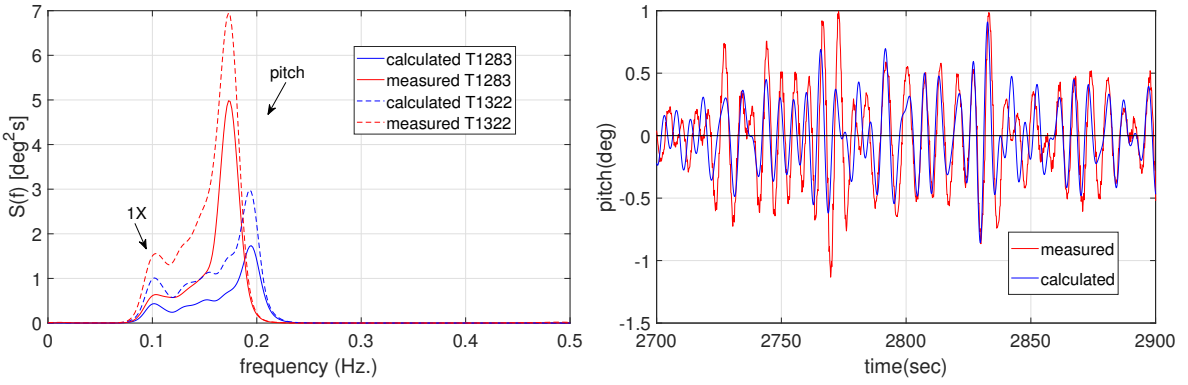

Figure 10: Pitch PSD (left) and time-domain comparison from T1283 (right)

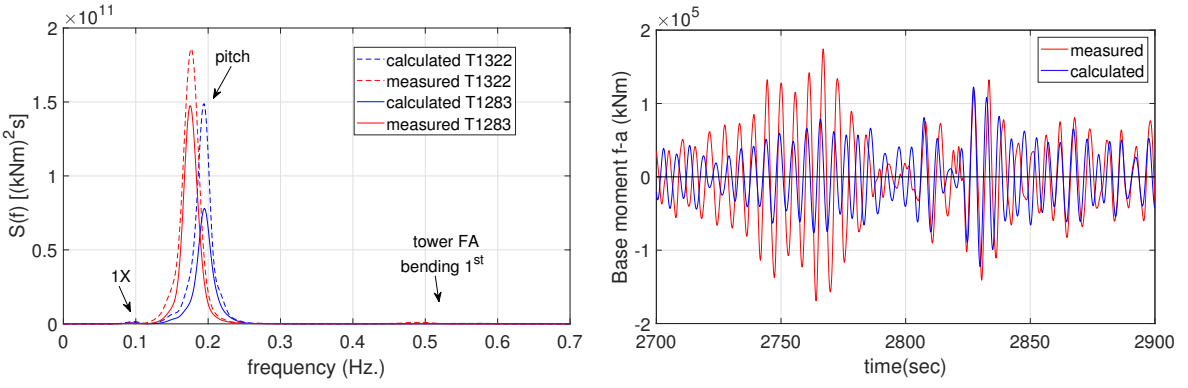

Figure 11: Tower fore-aft bending moment PSD (left) and time history comparison from T1283(right)

barely visible in 4m-wave case. Similar to the pitch response, the difference in the calculated and measured pitch natural frequencies resulted in phase shifts in fig. 12(b) but similar tension levels. Measured and calculated T3 magnitudes are very close to T1 but with 180 degrees of phase shift (blue dash lines). More information on T3 is given in the response statistics.

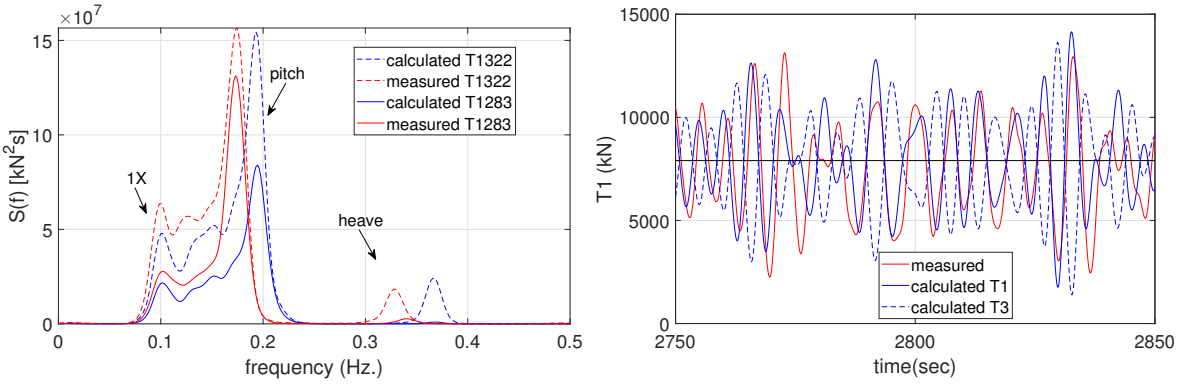

Figure 12: T1 PSD (left) and time history comparison from T1283 (right)

Heave spectral plots for 4m-wave (solid lines) and 6m-wave cases (dashed lines) are given in figure 13(a) with

peaks indicating each component of the response. The calculated response from the numerical model is composed of peaks around the peak wave frequency and heave natural frequencies of the platform. On the other hand, a component around the platform surge natural frequency, and a component at 1.58 Hz. is detected in the measured heave response from the physical model. Moreover, the high-frequency component is noticed in all the measured responses, including the wave gauges and force gauges from free decay tests; regular and irregular wave tests. The source of the high-frequency component can not be addressed to a specific target due to lack of information but is estimated to be either a measurement system issue since the magnitudes are very small or due to a loose connection between the tower and the platform or between the platform and the pontoons. Further information is available in Vardaroglu (2021). The 6m-wave case resulted in a relatively higher response compared to the 4m-wave cases. A close look at the zero-mean heave time history from T1283 is given in fig. 13(b), where the measured response is represented with three different colors (grey, green and red): Grey data series represents the total response that indicates a maximum heave of 15 cm in the physical model. Green and red data series are the filtered measured heave responses. Comparison of the red and blue lines shows that the measured and calculated heave responses are extremely small, which is the expected behavior from TLPs.

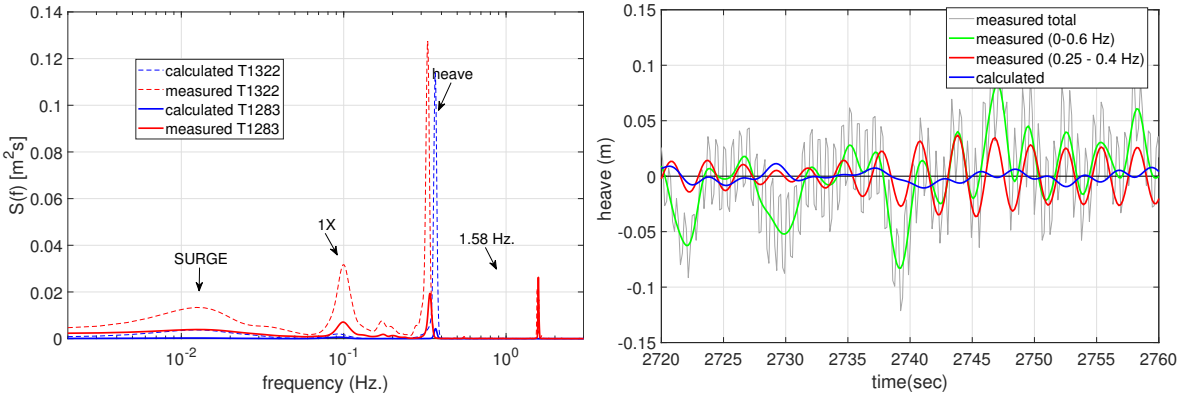

Figure 13: Heave PSD (left) and time history comparison from T1283 (right)

Statistics of the measured and calculated responses under 4m-wave and 6m-wave cases are given in Tables 5 and 6 for mean value and standard deviations. Related values are calculated from the time histories of the surge, heave, pitch, tendon tensions, and tower base fore-aft moment. The difference between the numerical and physical model response is divided by the physical model value and given in percentages. It should be noted that 4m-wave cases are represented here only with test T1283 since the corresponding results from test T1284 and test T1321 are very close to the T1283 values.

Table 5 shows the zero-mean values. Accordingly, the numerical model surge responses are 27% and 6% smaller compared to the physical model. In the physical model, mean heave and mean pitch values are not initially zero, which is believed to be a measurement system issue. Mean tendon tensions are in good agreement in the measured T1283 but 5268 kN less than the reference pretension value in the case of T1322. In the numerical model, the zero-mean value of total tendon tension is 31510 kN for T1283 and 31549 kN for T1322 which is 39 kN more than the pretension value. Tower base bending moment mean values are close to zero in the numerical and physical model.

According to table 6, surge standard deviation is 2% smaller in the numerical model for T1322 and 18% smaller for T1283. This result confirms the inference obtained from figure 9. The standard deviation of T1 from T1322 and T3 from T1283 is calculated the same as in the physical model. 5% smaller T1 and 3% larger T3 are calculated in T1283 and T1322, respectively. Side tendon tension deviations are relatively small compared to T1 and T3 and are not presented in the table. Maximum 275 kN of difference is obtained between the calculated and measured values. Moreover, heave and pitch responses are extremely small, which is the expected case in TLPs. Consequently, 24% smaller tower base bending moment standard deviation is obtained with the numerical model compared to the physical model, which is sourced to the different resonance behavior of two models at platform pitch natural frequency.

Table 5
Mean values of the numerical and physical model responses

	T1283			T1322		
Response	Physical	Numerical	Diff.(%)	Physical	Numerical	Diff.(%)
Surge(m)	0.40	0.29	-27	0.63	0.59	-6
Heave(m)	-0.66	-0.01	-	-0.89	-0.02	-
Pitch(°)	1.37	0.00	-	1.50	0.01	-
Mbyy (kNm)	655	-1420	-	256	-1382	-
T1 (kN)	7612	7858	3	6494	7828	21
T2 (kN)	8083	7927	-2	6710	7985	19
T3 (kN)	7750	7907	2	6710	7975	19
T4 (kN)	7662	7828	2	6278	7770	24

Table 6
Standard deviations of the numerical and physical model responses

	T1283			T1322		
Response	Physical	Numerical	Diff.(%)	Physical	Numerical	Diff.(%)
Surge (m)	0.74	0.61	-18	1.10	1.08	-2
Heave (m)	0.04	0.01	-	0.08	0.05	-
Pitch (°)	0.41	0.28	-	0.54	0.39	-
Mbyy (kN-m)	6.2E4	4.7E4	-24	7.5E4	6.4E4	-15
T1 (kN)	2207	1972	-11	2874	2825	-2
T3 (kN)	2080	1982	-5	2766	2845	3

6. Conclusions

In this paper, the results of a numerical approach that aims to predict the motion response of a TLP wind turbine are discussed. The numerical model is calibrated and compared with physical test measurements obtained from a previous test campaign conducted in 2012. Physical model information, wave basin set up, and test information is obtained from the related references. Open-source tools are used for hydrodynamic and motion response analyses. The dynamic response of the TLP FWT model is compared with the physical model response from free- decay, regular and irregular wave tests and discussed in time and frequency domains.

The physical model was designed with Froude scaling of all the components, including the rotor and the blades. Accordingly, the static horizontal load was applied at the nacelle level employing a pulley system. Consequently, the comparison of the numerical and physical models is limited to the cases under wave-only loading. Extremely stiff behavior of TLP and the scaled physical model yielded very small measurements in model scale. The precision of the numerical analyses is increased by using the measured wave gauge measurements as wave elevation time series. Followingly, a comparison of the responses under regular and irregular waves shows good agreement between the two approaches. On the other hand, discrepancies are observed in the measurements from the physical model tests. 17% smaller natural period in surge DoF is extracted from the physical model in the sway decay test compared to the numerical model. Response comparisons under regular wave cases revealed a physical test with off-trend response in all the RAO computations.

On the other hand, smaller heave and pitch responses are obtained under irregular waves with the numerical model compared to the physical model, which is the consequence of the difference in the platform pitch natural periods. A high-frequency component that dominates the heave is observed in all the measured quantities from the physical scaled model and estimated as noise due to a possible loose connection.

Besides the limits and discrepancies of both approaches, the two approaches also complement each other. Hydrodynamic damping in the numerical model is tuned by the results of decay tests on the physical model. Linear damping is added to the numerical model, which corresponds to the viscous drag of the platform in surge and sway DoF, the structural damping in heave due to the vibration of the tendons.

It should be reminded that FWTs are subjected to wave and wind loads under harsh met ocean conditions. Response

of FWTS under simultaneous wind and wave loads can only be observed by considering a coupled approach in the numerical analyses and using an RNA that properly reflects the aerodynamic and aeroelastic properties of the prototype in the experimental model. Moreover, turbulent wind loads may excite the resonant response and should be taken into account in the design of FWTs. However, since the numerical model can't be validated against model scale test under turbulent wind actions, the cases under wind excitation are out of the scope of this study.

In conclusion, the numerical model used in this study is capable of predicting the motion response of the TLP wind turbine but should be equipped with the sum-frequency loads considering the relatively smaller natural periods of the TLPs in the literature. Comparison of numerical and physical responses addresses the uncertainties in physical model testing of TLP wind turbines. Moreover, apart from the difficulties of TLP physical model tests, a future study that covers resonance motions in a wider regular wave period is suggested. Pitch natural periods obtained from the numerical (5 s) and physical model (5.5 s) are in the incident wave zone. Accordingly, the structural design should be checked by considering the reference tendon stiffness values since the first-order wave loads may dominate and excite resonant motions in platform pitch DoF. Cases under wind excitation need to be evaluated to investigate the effect of wind excitation on the response.

7. Acknowledgments

The experimental results used in this research were produced within a project funded under the Integrated Infrastructure Initiative HYDRALAB IV of EU FP7. The release of the data is acknowledged.

CRediT authorship contribution statement

Mustafa Vardaroglu: Conceptualization, Methodology, Numerical model & computations, Writing - original draft, Review &editing. **Zhen Gao:** Conceptualization, Methodology, Review &editing. **Alberto Maria Avossa:** Conceptualization, Methodology, Review &editing. **Francesco Ricciardelli:** Conceptualization, Methodology, Review &editing.

References

Armenio, E., 2014. Physcial model experiments on floating off-shore wind turbines. Ph.D. thesis. Università del Salento.

Armenio, E., D'Alessandro, F., 2013. Dynamic response of floating offshore wind turbines under random waves and wind action HyIV – DHI - 01 Offshore wave basin DHI Data Storage Report. Technical Report. Danish Hydraulic Institute.(DHI), Horshølm, DK (Denmark). Internal report.

Arnal, V., 2016. Drift force computation in nemoh: Far-field formula.

Babarit, A., Delhommeau, G., 2015. Theoretical and numerical aspects of the open source bem solver nemoh, in: 11th European wave and tidal energy conference (EWTEC2015).

Bachynski, E.E., 2014. Design and dynamic analysis of tension leg platform wind turbines. Ph.D. thesis. Norges teknisk-naturvitenskapelige universitet.

Bachynski, E.E., Moan, T., 2012. Design considerations for tension leg platform wind turbines. Marine Structures 29, 89–114.

Bir, G., 2005. User's Guide to BModes (Software for Computing Rotating Beam-Coupled Modes). Technical Report. National Renewable Energy Lab.(NREL), Golden, CO (United States).

Brodtkorb, P.A., Johannesson, P., Lindgren, G., Rychlik, I., Ryden, J., Sjö, E., et al., 2000. Wafo-a matlab toolbox for analysis of random waves and loads, in: The tenth international offshore and polar engineering conference, International Society of Offshore and Polar Engineers.

Buisson, F., Rongére, F., 2017. Meshmagick. last accessed 5.

Chakrabarti, S.K., 1987. Hydrodynamics of offshore structures. WIT press.

Chopra, A.K., 2007. Dynamics of structures. Pearson Education India.

Faltinsen, O., 1993. Sea loads on ships and offshore structures. volume 1. Cambridge university press.

Geuzaine, C., Remacle, J.F., 2009. Gmsh: A 3-d finite element mesh generator with built-in pre-and post-processing facilities. International journal for numerical methods in engineering 79, 1309–1331.

Greco, M., 2012. Tmr 4215: sea loads lecture notes. Trondheim, Norway: Dept. of Marine Technology, Norwegian University of Science and Technology , 77–80.

Hall, M., 2015. MoorDyn user's guide. URL: http://www.matt-hall.ca/files/MoorDyn-Users-Guide-2017-08-16.pdf. (accessed January 10, 2020).

Jonkman, J., 2010. Definition of the Floating System for Phase IV of OC3. Technical Report. National Renewable Energy Lab.(NREL), Golden, CO (United States).

Jonkman, J., 2013. Overview of the elastodyn structural-dynamics module. Natl Renewable Energy Lab .

Jonkman, J., Butterfield, S., Musial, W., Scott, G., 2009. Definition of a 5-MW reference wind turbine for offshore system development. Technical Report. National Renewable Energy Lab.(NREL), Golden, CO (United States).

Jonkman, J., Matha, D., 2010. Quantitative comparison of the responses of three floating platforms. Technical Report. National Renewable Energy Lab.(NREL), Golden, CO (United States).

Jonkman, J.M., 2007. Dynamics modeling and loads analysis of an offshore floating wind turbine. Technical Report. National Renewable Energy Lab.(NREL), Golden, CO (United States). .

Jonkman, J.M., Robertson, A., Hayman, G.J., 2014 (accessed October 16, 2020). HydroDyn User's Guide and Theory Manual. URL: https://raf-openfast.readthedocs.io/en/docs-hydrodyn_manual/source/user/hydrodyn/index.html.

Kvittem, M.I., 2014. Modelling and response analysis for fatigue design of a semi-submersible wind turbine. Ph.D. thesis. NTNU.

Lee, C.H., Newman, J.N., 2006. Wamit user manual. WAMIT, Inc , 42.

Masciola, M., 2015. Static configuration. https://map-plus-plus.readthedocs.io/en/latest/. Accessed: 2021-07-17.

Masciola, M., 2016. Map++ Documentation Release 1.15. Technical Report. Technical report, National Renewable Energy Laboratory-NREL.

Matha, D., 2010. Model development and loads analysis of an offshore wind turbine on a tension leg platform with a comparison to other floating turbine concepts: April 2009. Technical Report. National Renewable Energy Lab.(NREL), Golden, CO (United States).

Moriarty, P.J., Hansen, A.C., 2005. AeroDyn theory manual. Technical Report. National Renewable Energy Lab., Golden, CO (US).

NREL, . Openfast v2.5.0 documentation. https://openfast.readthedocs.io/en/latest/index.html. (Accessed: 2021-07-19).

Oguz, E., Clelland, D., Day, A.H., Incecik, A., López, J.A., Sánchez, G., Almeria, G.G., 2018. Experimental and numerical analysis of a tlp floating offshore wind turbine. Ocean Engineering 147, 591–605. URL: https://pureportal.strath.ac.uk/en/publications/experimental-and-numerical-analysis-of-a-tlp-floating-offshore-wi.

Penalba, M., Kelly, T., Ringwood, J., 2017. Using nemoh for modelling wave energy converters: A comparative study with wamit .

Philippe, M., Combourieu, A., Peyrard, C., Robaux, F., Delhommeau, G., Babarit, A., 2015. Introducing second order low frequency loads in the open-source boundary element method code nemoh, in: 11th European Wave and Tidal Energy Conference (EWTEC2015).

Riefolo, L., Vardaroglu, M., Avossa, A.M., 2018. Experimental tests on the wave-induced response of a tension leg platform supporting a 5 mw wind turbine, in: Conference of the Italian Association for Wind Engineering, Springer. pp. 599–612.

Standing, R., Brendling, W., Wilson, D., 1987. Recent developments in the analysis of wave drift forces, low-frequency damping and response, in: Offshore technology conference, OnePetro.

Thomsen, J.B., 2017. Validation of Mean Drift Forces Computed with the BEM Code NEMOH. Technical Report.

Tomasicchio, G.R., D'Alessandro, F., Avossa, A.M., Riefolo, L., Musci, E., Ricciardelli, F., Vicinanza, D., 2018. Experimental modelling of the dynamic behaviour of a spar buoy wind turbine. Renewable Energy 127, 412–432.

Tomasicchio, G.R., D'Alessandro, F., Musci, E., Fonseca, N., Mavrakos, S.A., Kirkegaard, J., Katsaounis, G.M., Penchev, V., Schüttrumpf, H., Wolbring, J., et al., 2014. Physical model experiments on floating off-shore wind turbines, in: Proceedings of the HYDRALAB IV Joint User Meeting, Lisbon.

Tracy, C.C.H., 2007. Parametric design of floating wind turbines. Ph.D. thesis. Massachusetts Institute of Technology.

Vardaroglu, M., 2021. Dynamic Behavior of Tension Leg Platform Floating Wind Turbines. Ph.D. thesis. Università degli Studi della Campania "Luigi Vanvitelli".

Vardaroglu, M., Gao, Z., Avossa, A., Ricciardelli, F., 2020. Numerical modelling of the mit/nrel tlp wind turbine and comparison with the experimental results, in: Journal of Physics: Conference Series, IOP Publishing. p. 012015. doi:10.1088/1742-6596/1669/1/012015.

Veritas, D.N., 2010a. Global performance analysis of deepwater floating structures. Høvik: Det Norske Veritas .

Veritas, D.N., 2010b. Recommended practice dnv-rp-c205: environmental conditions and environmental loads. DNV, Norway .